2014-01-01

Design Of Three Different Particle Size Distributions In Silver Paste Through Computer Simulation For Higher Electrical Conductivity

Kyungdeok Jang
University of Texas at El Paso, kjang@miners.utep.edu

DESIGN OF THREE DIFFERENT PARTICLE SIZE DISTRIBUTIONS IN SILVER PASTE THROUGH COMPUTER SIMULATION FOR HIGHER ELECTRICAL CONDUCTIVITY

KYUNGDEOK JANG

Department of Metallurgical and Materials Engineering

APPROVED:

Lawrence E. Murr, Ph.D., Chair

Stephen W. Stafford, Ph.D.

Russell R. Chianelli, Ph.D.

Charles Ambler, Ph.D.
Dean of the Graduate School

Dedication

I dedicate this thesis to my family and Jiyoung Kim. Without their support and unconditional love, the completion of this work would not have been possible.

DESIGN OF THREE DIFFERENT PARTICLE SIZE DISTRIBUTIONS IN SILVER PASTE THROUGH COMPUTER SIMULATION FOR HIGHER ELECTRICAL CONDUCTIVITY

by

KYUNGDEOK JANG, B.S.

THESIS

Presented to the Faculty of the Graduate School of

The University of Texas at El Paso

in Partial Fulfillment

of the Requirements

for the Degree of

MASTER OF SCIENCE

Department of Metallurgical and Materials Engineering

THE UNIVERSITY OF TEXAS AT EL PASO

DECEMBER 2014

Acknowledgements

I would like to express the deepest appreciation to my advisor, Dr. Lawrence E. Murr who is great scholar in metallurgical and materials science, for his excellent guidance, patience, and financial support. I applied many experimental approaches and techniques that I learned from his class on this thesis. The experience studying and working with you is an enjoyable time period which I will cherish forever.

Also, I am grateful to Mr. David Brown and Dr. Yirong Lin's research group members, Dr. Yirong Lin, Mr. Gerardo Rodriquez, and Mr. Shuvo Mohammad, who allow me to use lab facility and gave lots of help, and as well as Printing nano engineering lab for using conductivity meter. Thanks are also due to Dr. Stephen W. Stafford and Dr. Russell R. Chianelli for serving on the committee.

Finally, I would like to thank Mr. Francisco Andrade, Mr. Ubaldo Robles, Mr. Seongik Hong, Ms. Jihyun Hwang, Mr. Seyeon Hwang, Ms. Ada Ortega, Mr. Aldo Vidaña, Mr. Cesar Sanchez, and Ms. Nubia Zuverza. They treated me like a family and brother, and gave me a lot of help in my abroad life, study, and research during two years. I couldn't have done it if it weren't for your help.

Abstract

In the field of printed electronics technology, researchers have tried to print highly conductive electrodes with fine width and height in order to manufacture high performance devices.

The purpose of this research is to print particle monolayer silver patterns which have better electrical conductivity than existing ones. The key idea of this experiment is to analyze silver inks with different sized particles. Let us consider a particle monolayer pattern printed with silver ink consisting of mono-sized particles. Inside of the pattern, there are some vacant spaces between the particles, which can lead to low electrical conductivity and discontinuity of the pattern. If smaller particles are put into the spaces in the silver ink of mono-sized particles, the pattern will have fewer vacant spaces, increasing electrical conductivity of the pattern.

Computer simulation was developed in order to calculate monolayer packing density of three different sized particles and each distribution ratio of the particles in a plain. There were some variables to be considered in the computer simulation, and they were optimized. Various packing density results with different particle size ratio were obtained from the computer simulation.

To verify the computer simulation results, three different kinds of silver inks were fabricated according to the computer simulation results, and then printed to see the particle monolayer packing density of the pattern and to measure the electrical resistivity. The printed pattern by using the silver ink which contains three different sized particles has higher packing density and less electrical resistivity compare to the other silver inks which contain two different sized particles and mono sized particles, respectively.

Table of Contents

List of Tables

List of Figures

Chapter 1
Introduction

1.1 Research Purpose

In the printed electronics research, one of the major issues is to make a printed electrode which has high electrical conductivity. The factors that affect electrical conductivity of the printed electrode are metal contents, impurities, and treatments of conductive ink. Most researches used conductive inks with mono-sized particles [1-3]. When a particle monolayer pattern is printed with mono-sized particles, there will be some vacancy in the pattern. This research focused on increasing the packing density in the printed monolayer pattern by filling the gaps with smaller particles based on the computer simulation results.

1.2 Research Background on Printed Electronics

1.2.1 Advantages of Printed Electronics.

When thinking about the electronics industry, people may think of some kind of computer processor or memory consisting of semiconductor chips and electronic circuits on silicon substrates. However, a new technology is arising, which is called printed electronics; it has recently entered the electronics market and has been growing in the past decade. A silicon substrate is not essential in this technology because of the low temperature treatment; therefore, this new technology can fabricate electronic devices on the various substrates using simple printing process.

Printed electronics refers to electronic devices or modules made by printing technology. Products are “printed” on plastic, paper, or other substrates using conductive inks. This technology has no limits in selecting substrates; therefore, it is possible to produce novel products such as flexible devices and wearable devices. Since a conductive ink is directly printed on the substrate, printing process does not require complex steps like photolithography process. Figure 1.1 shows comparison between standard photolithography and printed electronics process for making electric circuits. The photolithography process consists of complex steps: spreading materials, coating, masking, and etching. On the other hand, the printed electronics process consists of just printing and treatment. These simple steps reduce not only energy and cost in processing, but also waste materials and their treatment. Printed electronics technology has been widely researched for the commercialization, and for now this technology can over low-tech devices like printed antennas or solar cells [4, 5].

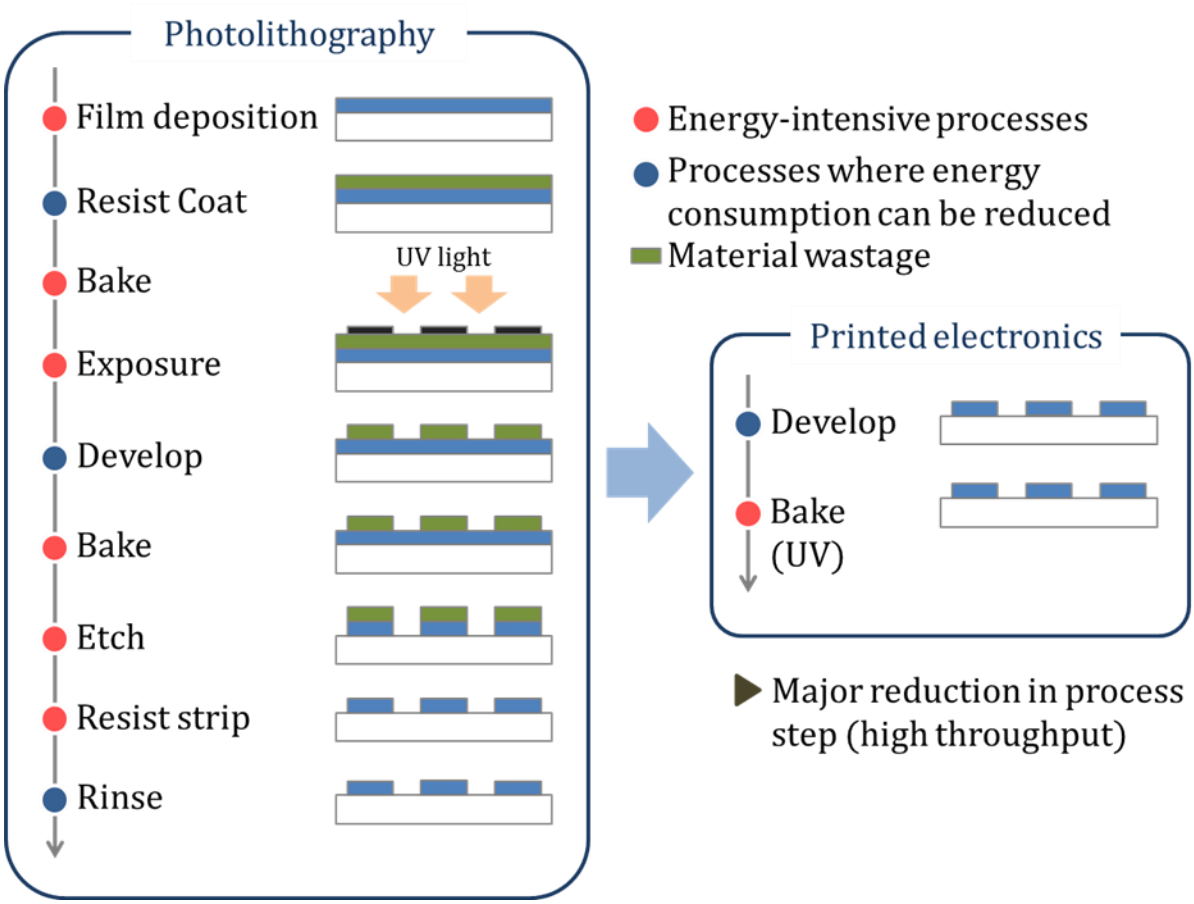

Figure 1.1 Comparison of Photolithography and Printed Electronics Processes [6].

1.2.2 Printing Methods.

Printed electronics technology can be classified according to printing equipment and materials technology. There were various printing technology methods in the initial stage of this research; however, researches are focusing on inkjet and roll-to-roll methods. Each printing method has both advantages and disadvantages. The major requirements for printing process are resolution, printing speed, and generality of printing materials. Specifications of each printing system are listed in Table 1.1.

Inkjet printing.

Inkjet printing processes form patterns just general printers print letters on paper. A fine droplet is injected through the nozzle and attached on the substrate. After the solvent is dried, solid components are fixed. The droplet diameter is around 10 to 90 picometers. The major parameter to determine the pattern resolution is the droplet size and wettability. This process easily can change the pattern design compared to other processes. However, inkjet printing has a slow printing speed. And it can only inject low viscous material like water. Also, more than a ten micron sized pattern resolution is an obstacle to apply to high-end devices with fine pattern.

Roll-to-roll printing.

Roll-to-roll printing is a process that forms a pattern continuously with a rotating rolled substrate. A concaved or convexed-blanket takes the ink then transfers the ink to the substrate. There are various kinds of roll-to-roll processes like: gravure, gravure offset, and reverse offset. Because the pattern is formed by a face-to-face process, major parameters of this process are pressure between roll and substrate, affination among roll-ink-substrate, printing speed, and temperature.

Table 1.1. Printing Systems and Their Features [7, 8].

Printing Technology	Thickness (μm)	Resolution (μm)	Viscosity (cP)	Throughput (m^2/min)	Resistration (μm)
Inkjet Printing [7]	<0.5	20~50	1~30	0.01~0.5	5~20
Gravure Printing [7]	0.8~10	75	50~200	60	>10
Gravure Offset Printing [7]	0.5~3	10~50	40,000~100,000	5~30	>10
Flexo Printing [7]	0.8~2.5	80	50~500	10	<200
Reverse Offset Printing [7]	0.1~1	>3		2~3	
Microdispensing [8]		>50	1~1,000,000	0.01~0.5	

The printing speed in this process is faster than inkjet printing, and some methods can print at a high resolution pattern (Table 1.1). However, this process does not print high viscous material (~200,000cPs).

Microdispensing.

The microdispensing method dispenses ink from a nozzle by air pressure, oil pressure, or a screw. It can dispense high viscous materials as far as a million centipoises. This printing method resembles drawing; therefore, it can easily make three-dimensional shapes with high viscous materials. Also, it can control injection quantity as far as 10 to 90 picoliters. However, the more viscous material the more pressure is required. Therefore, there is a limitation of pattern size up to 50μm [7]. Compared with roll-to-roll processes, it has a bad printing speed [8].

1.2.3 Materials for Printed Electronics.

Printed electronics technology began the after development of nanotechnology because of the physical properties of nano materials [9-10]. One of the important physical properties is the change of the melting point. As the gold particle size decreases the melting point decreases in a steady manner. Then, when it reaches a critical value approximately 5nm, the melting point decreases sharply. (Figure 1.2) [11]. Nano materials facilitate low temperature processes; therefore, it is possible to make organic-based electronic devices instead of traditional silicon-based devices. Also, organic based materials have flexible properties; therefore, it can be applied to the smart device market for flexible, foldable, and wearable devices.

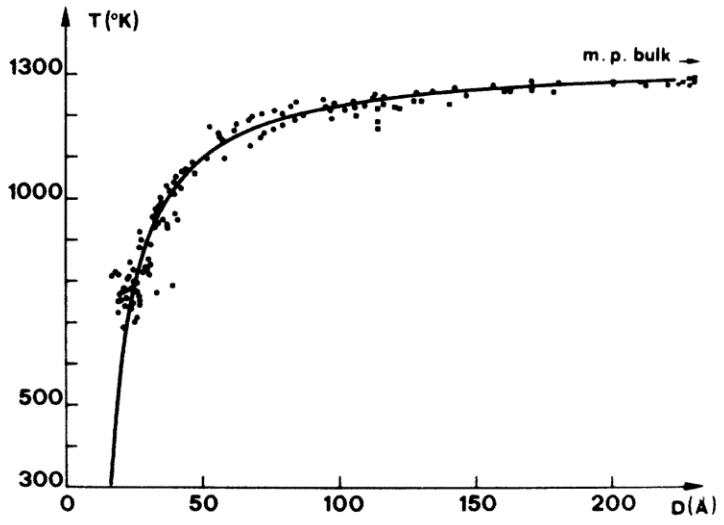

Figure 1.2. Experimental and Theoretical Values of the Melting-point Temperature of Gold Particles [11].

Material selection for printed electronics.

For the development of high-end devices using printed electronics technology, high electrical conductivity electrode printing is most important. The most conductive metals are gold, silver, and copper which can be made into nanoinks. Gold is the most stable metal among them, so it is safe to avoid oxidation (Table 1.2) [12]. It can be synthesized until few nanometers, and it can be synthesized to any required shape. However, gold is expensive, so it is not appropriate for use. For copper, when the particle size is smaller, oxidation stability will decrease. Therefore, copper nanoparticles are hard to apply to nanoinks because it tends to oxidize into copper oxide. The electrical conductivity of silver is best among the metals. Although its oxidation stability is less than gold, it is stable in its standard state. Also, it is fifty times cheaper than gold, so it is used the most in printed electronics materials.

Nanoink packing.

As noted above, to make high electrical conductivity printed electronics devices, not only is it important to use high electrical conductive materials, but the printing process is also important. Figure 1.3 shows a future roadmap of printed electronics technology [6]. For producing printed solar cells, displays, memories, and computer CPUs by printed electronics technology, it is essential to fabricate high conductive electrodes.

The major factors that effect nanoinks' conductivity are particle shape [13], size [14], purity [15], contact resistance [16], and packing density [17-21]. If the nanoparticles' packing density is not enough in the nanoink, it is quite probable that the nanoparticles in the electrode after printing will not contact each other. This causes low electrical conductivity and even no conductivity. Therefore, it is important to increase particle density in nanoinks.

Nanoinks for the printed electronics research usually contain mono-sized nanoparticles [1-3]. Assuming a particle monolayer printed pattern, the theoretical packing density of a cross-sectional area is 78.5%. If smaller sized particles are added into the pattern and fill the space, it is expected to have better electrical conductivity. Amert (2010) did the experiment that produced silver electrodes using two different sized particles getting better electrical conductivity [17]. He developed a computer simulation for monolayer particle packing. The result was only a 45% packing factor using mono-sized particles, and 66% when adding five times smaller particles. Electrical conductivity was 18.5% of the bulk conductivity when using mono-sized particles and 47% when using different sized particles. However, 30% of space still remains in the area; therefore, if smaller sized particles are added, more electrical conductivity can be expected.

Table 1.2 Gibbs Standard Free Energy for Copper, Gold, and Silver Oxides and Partial Pressure of Oxygen Required to Stop Oxidation at 25℃ [12].

Metal Oxides	$\Delta G^0_{f,25}, cal/mol$	P_{O_2}, atm
CuO	-30,400	2.60×10^{-45}
AuO_2	48,000	1.58×10^{35}
Ag_2O	2,600	6.51×10^{3}

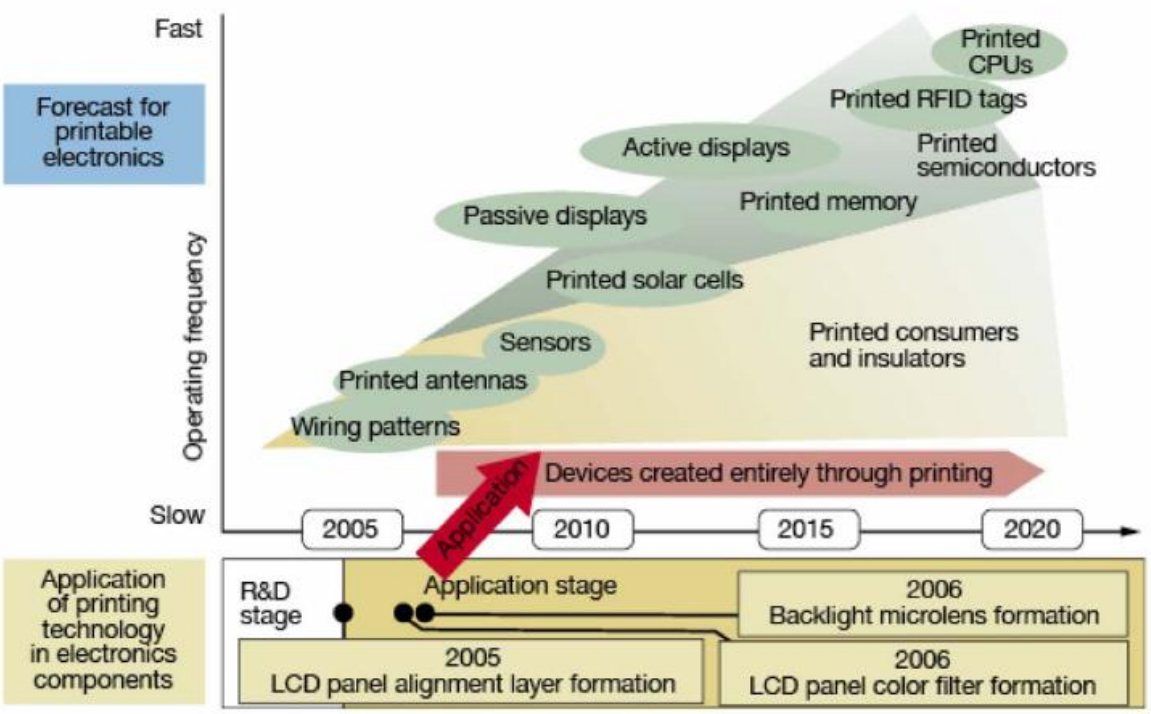

Figure 1.3 Technology Road Map of Printed Electronics [6].

Chapter 2

Computer Simulation for Nanoparticles Packing in Particle Monolayer

2.1 Introduction

Several studies have been performed in order to measure the exact amount of vacant space available for particle packing [22-23]. Amert (2010) developed a computer simulation to calculate a Two Dimensional Packing Factor (2D-PF): covered area by circle/total area of domain, % [17]. This is achieved by packing the ink's nanoparticles (NPs) in a computer simulation. Amert's (2010) study suggests that the highest 2D-PF is calculated when the diameter of the particles is at maximum one-tenth of the side of the domain. Therefore, using two different sized particles to calculate the 2D-PF was adequate. When the size ratio of the two particles is six, a 66% 2D-PF is obtained [17].

A simulation space can generate at most 2.5×10^9 particles, but a single computation experiment takes vast amounts time to calculate. The desktop computer (10 Million of Floating Point Operations Per Second (MFLOPS): 10^7 times per second) used in the simulation program cannot compute large amounts of data easily, and as the particle's radius decreases, it becomes more difficult for the computer to give an accurate 2D-PF value. The desktop computer can take up to more than a week to generate particles and analyze the data [24]. To reduce the simulation time, this current study used a supercomputer to process a large amount of data. Moreover, a third particle was added in the packing process expecting to increase the electrical conductivity. The purpose of this study is to increase the conductivity of printed electrode. To do this, a tertiary packing was attempted with a simulation program using a supercomputer.

2.2 Simulation Program Development

The Supercomputer SUN Blade 6048 (Figure 2.1) is the property of the KISTI (Korea Institute of Science and Technology Information). The supercomputer was coded with a different operation system from the desktop computer simulator to perform the current study.

Figure 2.1. Sun Blade 6048.

Table 2.1. Specifications of SUN Blade 6048 Super Computer.

Classification	Content
Model	SUN Blade 6048
Blade node	188 (Computing) 24TFlops(Rpeak)
CPU	AMD Opteron 2.0GHz 16(Node) 3,008(the whole)
Memory	32GB(Node)
Storage	207TB(Disk) 422TB(Type)
Network between node	Infiniband 4X DDR

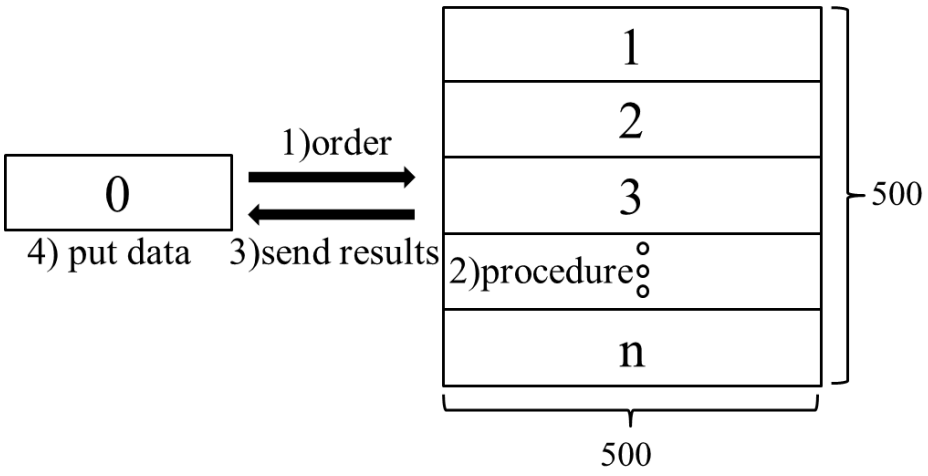

Figure 2.2. Skeleton of Computing System of the Supercomputer Simulator.

Figure 2.2 shows a rough computing system of the simulator. By using n-CPUs, the supercomputer will code programs in the simulation and will process large amounts of data faster than the desktop computer. The program was designed using C-language and Message Passing Interface.

From the metallurgical point of view, spherical particles have a low surface energy. Most metal powder is used in spherical shape because it is thermodynamically favorable. The main purpose of this research is to manufacture metal conductive ink and apply computational concept to general applications. Therefore, the particle shape was assumed to be spherical.

The supercomputer simulator uses a process in which it selects particles randomly in the domain while considering the properties of real particles in the media. The system will work by having a CPU 0 arranging the received data and giving orders to the other CPUs. The rest n-1 CPUs will control each n-1 divided virtual space. The maximum number of CPU in this experiment is 11 including CUP 0. In this case, each space is divided 500 by 50 (unit less), and stored in a linked list method. This allows for a parallel processing of the divided space (not a linear process), which is faster at producing data.

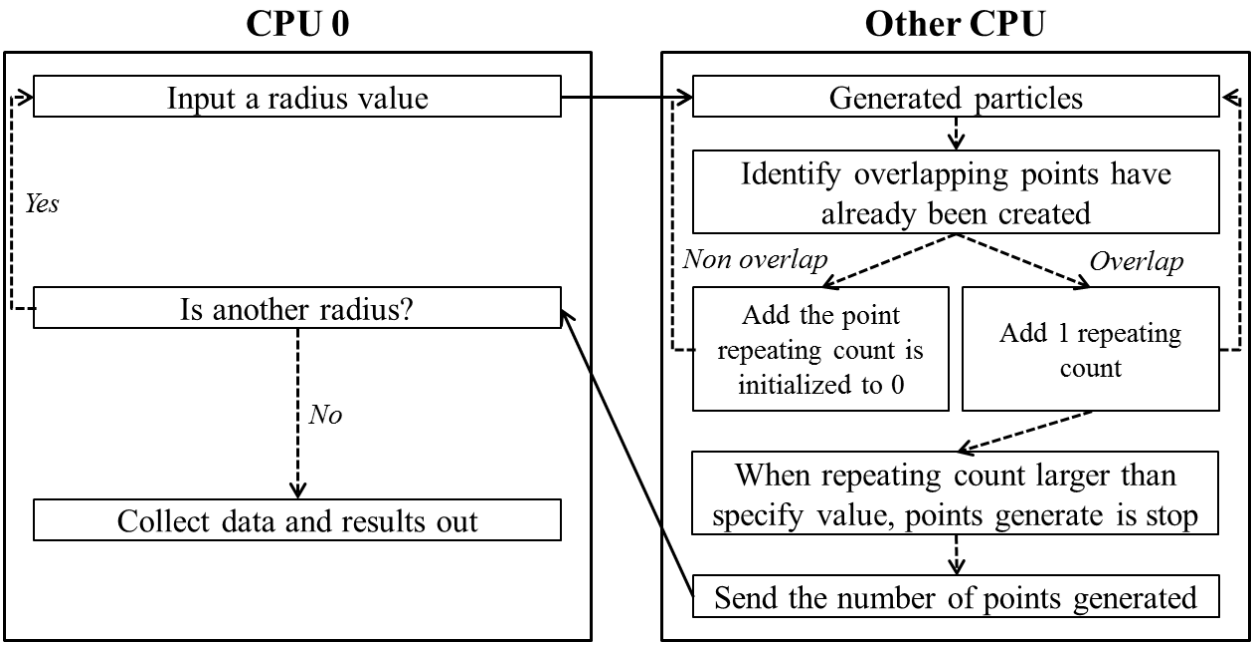

Figure 2.3. Algorithm of Supercomputers Simulating System.

Figure 2.3 illustrates the algorithm of the simulators' computing system. The simulation process starts by setting the simulating domain 500 by 500 (unit less). Subsequently, CPU 0 will transmit the radius of the biggest size particle and order the other n-CPUs to generate particles while taking into consideration the nanoparticle's physical properties.

Each CPU generates particles using an input Repeating Count (RC) value. These values start at 0. When an existing particle overlaps a new particle is generated, the new particle is removed, and the RC value adds 1. When the RC value reaches a designated number, the CPUs stops generating particles, then a new process starts and the RC value is initialized. Once the particle generates by input RC value, the CPUs will carry out the next process. First, each CPU generates particles and transmits the coordinates of the particles in the boundary of the domain to the main CPU (CPU 0). When the particles generate in the boundary, they may overlap with each other on that boundary. As a result, CPU 0 distributes to each CPU the particles in the boundary

from the other CPUs, this is to prevent the overlapping of coordinates. For example, if some particles overlapped between CPU 2 and CPU 3, CPU 0 will receive the data from both CPUs and will distribute the data of CPU 2 to CPU 3, and data from CPU 3 to CPU 2. Each CPU will check whether there are overlapping particles, if they do not overlap they will transmit the data with its domain to CPU 0. When CPU 0 acquires the data, it distributes data to the rest of the CPUs, and they store the data. After finishing all processes, all the CPUs transmit the final data of generated particles to CPU 0, where it will add all received data. Subsequently, the whole process is performed again in an empty place in the domain where particles have not generated and shows the result. To verify the data generated by the supercomputer, we performed a computation experiment under the same conditions used for Amert's (2010) data [17].

2.3 Procedures

2.3.1 Verifying The Program Used for a Supercomputer.

To see whether the data from the program used for a supercomputer has the same results and tendency with the data from the desktop computer, a binary packing simulation was conducted using the supercomputer. The large diameter of a particle was 25 and the small ones were 12.5, 8.3, 5, 2.5, and 1.7. The Repeating Count was set at 1,000 and two CPUs were used. The results are shown in Figure 5, and the reliability of the program for the supercomputer was verified.

2.3.2 Setting The Repeating Count.

As we increase the Repeating Counts, the more frequently the simulator finds void space, thus obtaining a higher Packing Factor. Since room for the simulation is limited, setting an overly high Repeating Count will cause longer times of operations. In this computation experiment, we used equal diameter particles, six CPUs, and established Repeating Counts at 100, 1,000, 5,000, 7,500 and 10,000.

2.3.3 Setting The Number of CPU's.

The task of the CPUs is to divide each space and to perform parallel operations to analyze the data acquired. As we increase the amount of CPUs used, we can accelerate the operation process. By having each CPU execute the operations in their domain, we can apply the input Repeat Count separately, achieving a higher Packing Factor with smaller deviation. However, if a particle's diameter is larger than the width of the divided domain as in Figure 4, the number of overlapping particles will increase and operations will become more complex.

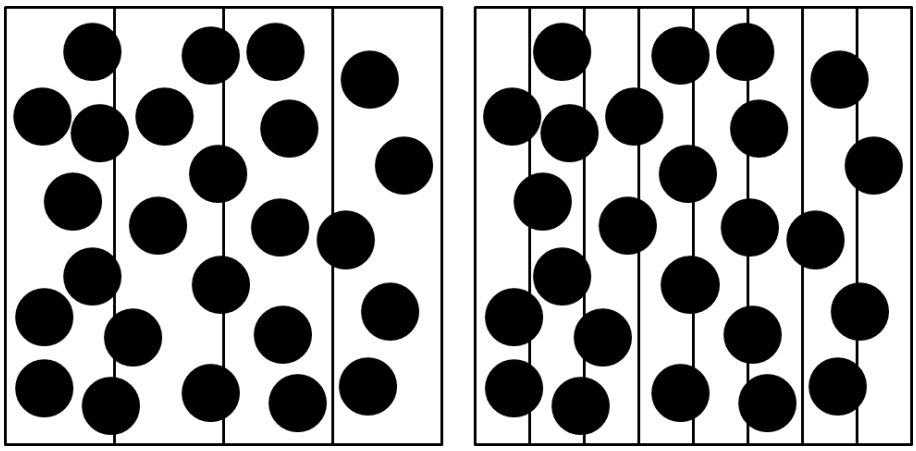

Figure 2.4. Comparison of the Number of Overlapping Particles on Boundary according to the Number of Divided Space.

Figure 2.4 demonstrates an increase in the number of overlapping particles in the boundary with respect to the number of divided space. When dividing the space into four, 10 particles overlap on the boundary; if divided into eight, 25 particles overlap. As a result, the space width of each CPU control must be larger than the particles diameter. The large particle on this computation experiment is a size 50. Therefore, the number of CPUs must be less than eleven including the main CPU.

2.3.4 Setting Tertiary Packing Simulation.

In an earlier study, Amert (2010) obtained a 66% Packing Factor using binary packing [17]. Unfortunately, some voids still existed. On the other hand, when using tertiary packing simulation we achieve a higher Packing Factor by setting the ratio of the particles around 10. This is due to the possibility of additional packing of smaller particles in the remaining voids. When using tertiary packing simulation, the large particle diameter was 25. The intermediate particle diameters were 12.5, 10.0, 7.5, 5.0, and 2.5 (between 1/2~1/10 of 25) and the small diameters were 1.25, 1.00, 0.75, 0.50, and 0.25. By setting the Repeat Count to 1,000, using 11 CPUs and repeating each simulation 10 times, we can calculate the mean and the standard deviation of the particles.

2.4 Results and Discussion

2.4.1 Supercomputer vs. Desktop Computer Data Acquisition Comparison.

Figure 2.5 displays the results of the comparison of the simulation data of the supercomputer and the desktop computer under identical particle creation conditions. The data is the average of each operation performed ten times resulting in an identical tendency between both sets of data. The data demonstrates an increase in the supercomputer simulations Packing Factor resulting in a 5% deviation from the desktop computer. With this, the simulation results of the supercomputer are reliable.

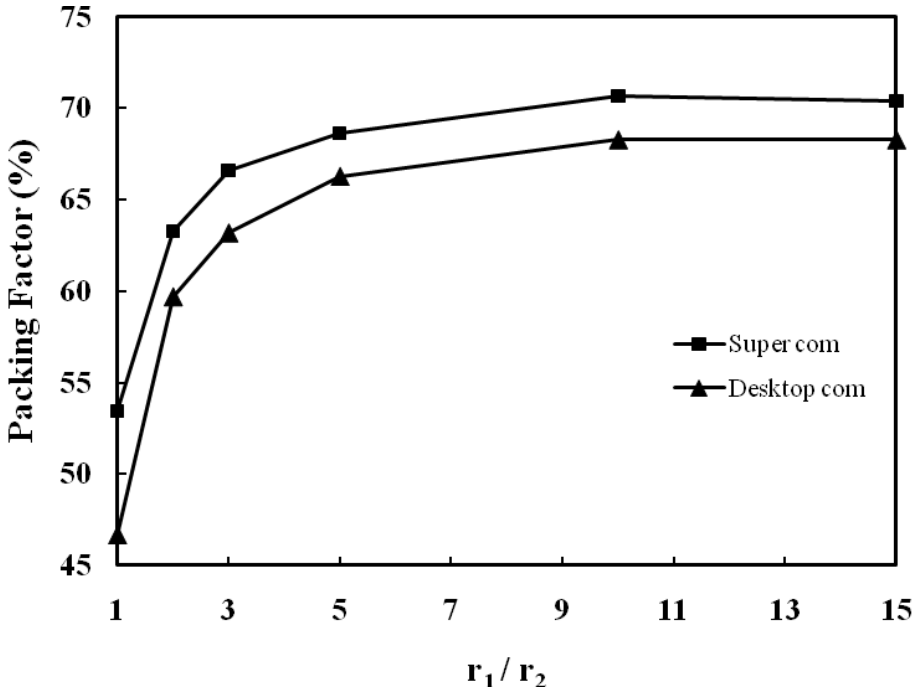

Figure 2.5. Comparison of Supercomputer and Desktop Data (Repeating Count: 1000, number of CPU: desktop 1, super computer 2).

2.4.2 Setting The Repeating Count.

As the Repeating Count increases, the probability of finding void space to fill decreases, allowing for a higher Packing Factor. Figure 2.6 shows the Packing Factor with respect to the Repeating Count. When the Repeating Count is greater than 5,000, all the Packing Factors are identical within a 0.6% deviation, meaning there is no more space for particles to be packed. If Repeating Counts are 100 and 10,000 the packing factor will increase as the size of the particles becomes smaller. However, since the vacant voids are filled with smaller particles the finding of more void space becomes more difficult, thus making a higher Repeating Count necessary to pack smaller sized particles.

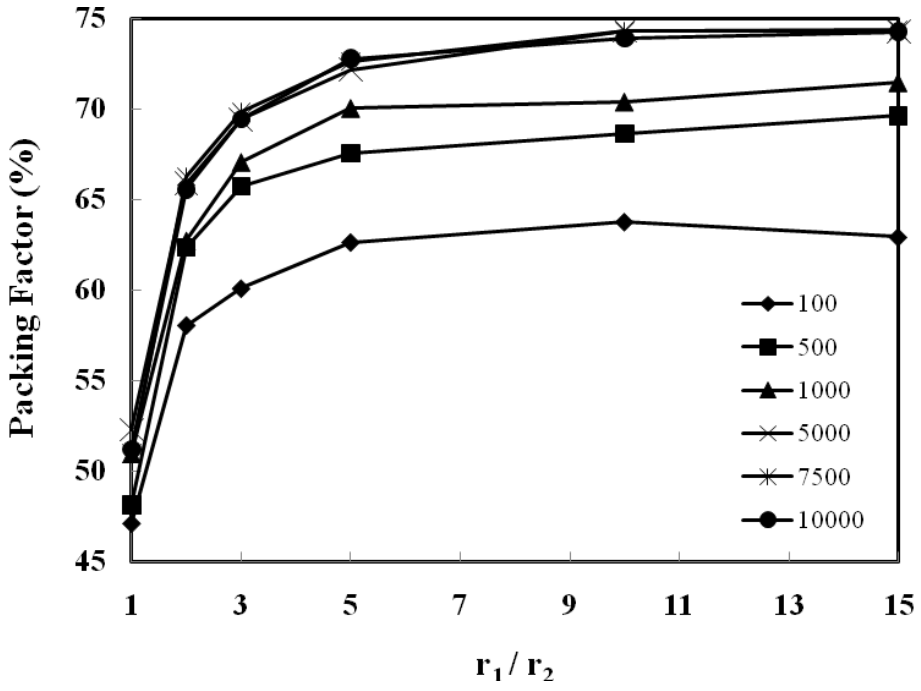

Figure 2.6. Changes in Packing Factor according to the Repeating Count (use 6 CPU).

2.4.3 Simulation according to the number of CPU.

As mentioned before, when using more CPUs to conduct the simulation the faster the operation time and the more accurate the results are for Packing Factor. This is due to applying a Repeat Count at each domain. Figure 2.7 illustrates the Packing Factor according to different combinations of CPUs, such as 2, 3, 6, and 11 CPUs not considering the main CPU 0. The CPUs that generate particles in the domain are CPUs 1, 2, 5, and 10. Table 2.2 shows the average time spent for the ten operations.

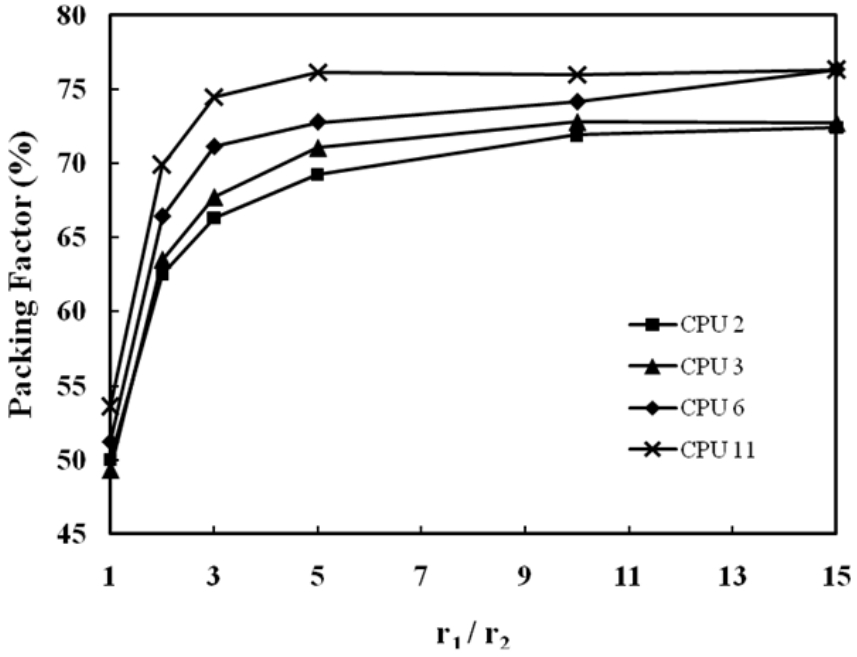

Figure 2.7. Packing Factor according to the Number of CPU's.

Table 2.2. Average of Operating Times (sec, 10 times).

Number of CPU / r_1/r_2	1	2	3	5	10	15
2	9	7	6	7	11	16
3	8	5	5	6	6	9
6	6	3	2	3	3	4
11	4	3	2	2	2	3

2.4.4 Tertiary packing simulation.

Depending on the Repeating Count setting and the number of CPUs, we can obtain various Packing Factors allowing for two randomly set values to be the desired results. Table 2.3 shows the result of all the packing simulations at each condition. The first three columns show the three particle sizes, the next three columns show the number of packing particles and their deviation in virtual space, and the last two columns show the Packing Factor and standard deviation for each simulated condition. Through this database, we can determine the sizes of the particles by using a quantitative experiment to obtain a volumetric ratio between the desired particles.

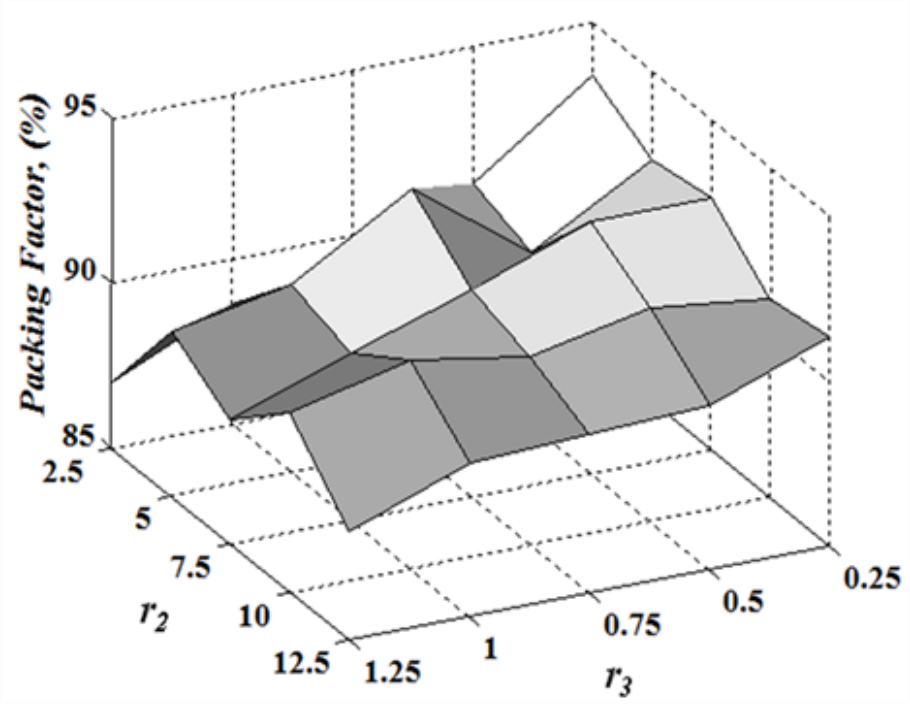

Figure 2.8. Simulation of Tertiary Packing.

The tertiary packing for high Packing Factor is simulated, and Figure 2.8 displays the results of the simulation in a three-dimensional graph drawn using the MATLAB program. When it comes to timing, we expected a long operational time when using particle sizes 25, 2.5, and 0.25, but surprisingly it timed out at 22 seconds, which was far shorter when compared to the desktop computer times. Next, when looking at our Packing Factors, we see that with particle sizes 25, 2.5, and 0.25 we obtain a high Packing Factor of 93.44%. When using 25, 2.5, and 1.25, we get the lowest Packing Factor measured to be 87%. All other Packing Factors were higher than 80%. From the data in Table 3, we see a tendency that as the Packing Factor increases the size ratio between adjacent particles (r1 between r2, and r2 between r3) increases.

One of the advantages of tertiary packing over binary packing is that more void space can be filled. There exists about 16% of void space at the highest packing result, which might be possible to fill with smaller particles if we can achieve a higher Packing Factor. However, this is difficult to apply to real printed electronics since the particle sizes are extremely small. For example, when making 30um pattern using nanoink, the size of the particles are 3um, 300nm, and 30nm. Therefore, it is not possible in practice to add smaller particles into the remaining void space, thus making quaternary particle packing futile.

Table 2.3. All Packing Simulation Results at Each Condition.

		Particle size			Number of particles(S.D.)						%	
R.C.	CPU	r_1	r_2	r_3	r_1		r_2		r_3		P.F.	S.D.
5000	11	25	2.5	0.25	60	(5.64)	3977	(209.98)	196566	(7985.32)	93.44	2.45
5000	11	25	5	0.25	58	(4.55)	960	(47.67)	216427	(5931.58)	92.33	2.03
5000	11	25	7.5	0.25	59	(4.97)	399	(28.00)	228469	(7053.63)	92.65	2.03
5000	11	25	10	0.25	55	(3.53)	225	(11.33)	246862	(6908.88)	91.06	1.66
5000	11	25	12.5	0.25	59	(5.40)	121	(16.71)	268546	(5813.72)	91.36	1.39
5000	11	25	2.5	0.5	58	(2.66)	4033	(139.09)	44130	(1031.44)	90.89	1.90
5000	11	25	5	0.5	54	(4.61)	1002	(52.83)	52501	(1687.83)	90.25	1.71
5000	11	25	7.5	0.5	60	(3.69)	402	(18.74)	55666	(1328.02)	92.65	1.84
5000	11	25	10	0.5	57	(3.54)	224	(17.93)	59190	(966.92)	91.49	1.68
5000	11	25	12.5	0.5	58	(3.74)	122	(9.20)	65897	(2416.38)	90.01	1.53
5000	11	25	2.5	0.75	57	(4.76)	4044	(267.93)	17624	(920.76)	88.94	1.43
5000	11	25	5	0.75	62	(3.97)	929	(44.09)	21251	(797.87)	92.87	1.45
5000	11	25	7.5	0.75	60	(2.56)	388	(14.72)	23857	(590.21)	91.28	1.47
5000	11	25	10	0.75	57	(4.70)	222	(20.85)	25694	(674.92)	90.73	1.24
5000	11	25	12.5	0.75	58	(5.23)	122	(11.26)	28537	(923.89)	89.81	2.44
5000	11	25	2.5	1	58	(3.08)	4072	(158.73)	8735	(264.17)	88.63	1.60
5000	11	25	5	1	57	(5.50)	983	(52.65)	11762	(553.54)	90.69	2.33
5000	11	25	7.5	1	56	(5.12)	420	(31.81)	13299	(392.36)	90.11	1.64
5000	11	25	10	1	59	(4.96)	218	(13.03)	13920	(516.35)	91.31	2.26
5000	11	25	12.5	1	59	(3.53)	120	(9.34)	15695	(352.04)	89.66	1.58
5000	11	25	2.5	1.25	60	(3.37)	3947	(174.74)	4462	(206.20)	87.00	1.48
5000	11	25	5	1.25	57	(6.55)	987	(72.58)	7175	(321.26)	89.97	2.38
5000	11	25	7.5	1.25	54	(5.43)	426	(40.92)	8369	(231.07)	88.80	1.26
5000	11	25	10	1.25	59	(4.30)	217	(11.38)	8763	(259.80)	90.48	1.86
5000	11	25	12.5	1.25	57	(4.68)	121	(7.67)	10038	(262.03)	88.29	2.08
7500	6	25	1.7	-	62	(3.35)	7093	(349.23)			74.34	1.50
7500	6	25	2.5	-	63	(2.88)	3122	(144.95)			74.28	1.22
7500	6	25	5	-	63	(2.17)	728	(35.12)			72.61	1.06
7500	6	25	8.3	-	64	(2.80)	231	(15.67)			69.81	1.31
7500	6	25	12.5	-	63	(3.49)	85	(10.49)			66.27	0.85
7500	6	25	-	-	65	(3.67)	-	-			50.95	2.88
10000	6	25	1.7	-	62	(3.24)	7154	(359.92)			74.25	1.31
10000	6	25	2.5	-	62	(2.50)	3173	(111.34)			73.89	1.30

10000	6	25	5	-	64	(3.37)	725	(42.83)	72.77	1.51
10000	6	25	8.3	-	62	(2.25)	238	(10.52)	69.44	1.08
10000	6	25	12.5	-	61	(2.50)	89	(6.93)	65.57	1.46
10000	6	25	-	-	65	(3.82)	-	-	51.18	3.00
5000	2	25	1.7	-	63	(2.36)	6331	(343.85)	72.44	0.67
5000	2	25	2.5	-	63	(1.52)	2871	(80.82)	71.91	0.68
5000	2	25	5	-	61	(1.97)	683	(25.69)	69.25	0.80
5000	2	25	8.3	-	62	(2.63)	207	(18.48)	66.32	0.67
5000	2	25	12.5	-	63	(2.53)	66	(5.77)	62.51	1.38
5000	2	25	-	-	64	(1.64)	-	-	50.00	1.28
5000	3	25	1.7	-	62	(2.42)	6734	(236.91)	72.72	1.11
5000	3	25	2.5	-	63	(1.90)	3012	(96.77)	72.79	0.89
5000	3	25	5	-	64	(2.60)	660	(37.04)	71.05	0.98
5000	3	25	8.3	-	63	(2.67)	214	(15.53)	67.72	1.20
5000	3	25	12.5	-	62	(2.33)	75	(8.80)	63.51	0.66
5000	3	25	-	-	63	(2.18)	-	-	49.32	1.72
5000	6	25	1.7	-	65	(4.59)	7013	(381.95)	76.32	2.51
5000	6	25	2.5	-	61	(3.41)	3305	(113.39)	74.14	1.92
5000	6	25	5	-	62	(3.09)	775	(29.96)	72.78	1.58
5000	6	25	8.3	-	64	(3.02)	241	(14.37)	71.12	1.68
5000	6	25	12.5	-	62	(3.41)	93	(11.07)	66.43	1.61
5000	6	25	-	-	66	(2.82)	-	-	51.24	1.89
5000	11	25	1.7	-	56	(4.52)	8853	(417.82)	76.33	2.09
5000	11	25	2.5	-	56	(3.96)	4088	(202.48)	75.97	1.82
5000	11	25	5	-	59	(5.74)	958	(70.81)	76.15	2.41
5000	11	25	8.3	-	59	(4.80)	324	(18.09)	74.47	2.44
5000	11	25	12.5	-	59	(4.73)	121	(12.49)	69.92	2.03
5000	11	25	-	-	69	(3.61)	-	-	53.62	3.65

Chapter 3

Application of Simulation Results for Actual Practice

3.1 Introduction

In order to verify the results of computer simulation, three different sized particles were synthesized. Then inks were fabricated by using the aforementioned particles. Afterwards, the electrodes were printed by a modified screen printing method. Lastly, the electrical resistivity of each of the electrodes was measured after the sintering process.

3.2 Preparations for Silver Inks

3.2.1. Synthesis of Silver Particles.

Silver nitrate ($AgNO_3$, Chem-impex int'l Inc.), ascorbic acid ($C_6H_8O_6$, Chem-impex int'l Inc.), and ammonium solution (NH_4OH, Fisher chemical) were used to synthesize two different sized silver particles. For the smaller particles, 0.68g of silver nitrate was dissolved in 90ml of distilled water. Then 10ml of ammonium solution was added into the silver nitrate solution. Subsequently, 1.76g of ascorbic acid dissolved with 100ml of water was added into the silver nitrate solution. The reaction time is approximately ten minutes. Finally, the particles were cleaned with ethanol followed by a drying process inside a vacuum chamber. The intermediate sized particles were synthesized using the same conditions. However, ammonium solution was not added into the silver nitrate solution in this procedure.

The synthesized silver particles were characterized using scanning electron microscopy. The particle size distribution was calculated manually from the SEM micrographs.

3.2.2. Synthesis of Cu-Ag Core-shell Particles

Cu-Ag core-shell particles are copper particles coated with silver. These particles were synthesized using the electro-less plating method. This method is driven by the difference of electric magnetic forces (EMF) between copper and silver. Table 3.1 shows the difference between the EMF values of silver and copper. In order for this reaction to happen the EMF value of the core metal must be lower than the shell material. When a silver ion is placed with a copper metal particle, the silver ion will take an electron from the copper metal, converting the silver ion into silver metal. Concurrently, the copper metal ionizes. At the end of the reaction, reduced silver metal will completely cover the surface of the copper particle. Figure 3.1 shows a schematic representation of the synthesizing process for the Cu-Ag core-shell.

Table 3.1.EMF Value of silver and copper [12].

Metal/ion	EMF (volts SHE)
Ag/Ag+	0.799
Cu/Cu++	0.337

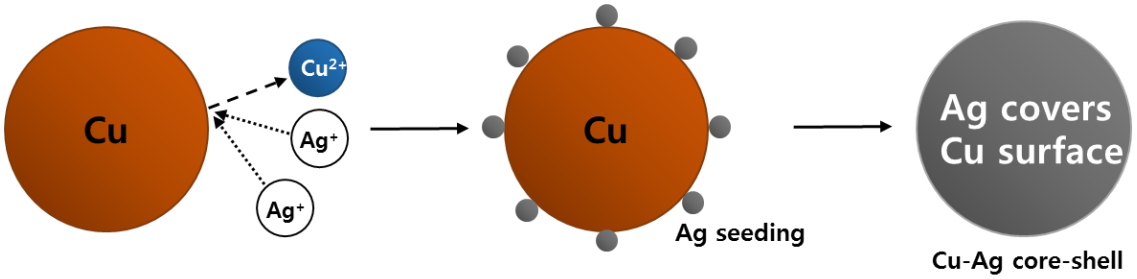

Figure 3.1. Schematic Process for Cu-Ag core-shell.

For synthesis of the Cu-Ag core-shell particle, copper powder with an average particle size of 30μm was used as the core material. Hydrazine monohydrate ($H_4N_2 \cdot H_2O$, Alfa Aesar) was used to pretreat copper powder. This helps get rid of copper oxide which might have existed on the surface of the copper particle. Silver nitrate and ammonium solution were used for electro-less plating.

After the pretreatment step, 1.5g of copper powder was put into 100ml of deionized water, then hydrazine ($[Cu]/[H_4N_2]=2$) was added into the solution to make it react for 10 minutes. The reduced copper powder was cleaned with ethanol at the end of the reaction. Next, 0.4g of silver nitrate was dissolved in 98ml of deionized water, and then 2ml of ammonium solution was added into the solution. Lastly, 0.38g of reduced copper powder was added into the solution and reacted for 5 minutes. Again, the Cu-Ag core-shell was rinsed with ethanol.

3.2.3. Fabrication of Silver Electrode.

In order to fabricate the silver inks, polyvinyl alcohol (PVA, Sigma-aldrich) and ethylene glycol ($C_2H_6O_2$, Fisher Scientific) were mixed with a ratio of 1:20 at 45℃ for 20 minutes. The mixed solution will then turn into a gel-like substance during cool down.

Three different kinds of silver inks were produced followed by the computer simulations. The first ink contained only bigger particles with the binder. The second ink contained both the bigger and the intermediate sized particles. Finally, the third ink contained all three of the particles made (the bigger, the intermediate, and the smaller sized particles).

Each ink was used to fabricate electrodes using the modified screen printing method. A scotch-type mask which had cut out 25mm by 1mm area was attached on the slide glass. The ink

was squeezed on one side of the mask using a razor. Figure 3.2 shows a schematic process of modified screen printing method used in this research. The mask was removed after the printing process. Printed electrodes were sintered at 500˚C for 2 hours. The surfaces of the sintered electrodes were observed by SEM, and their electrical resistivities were measured by resistivity meter (MCP-T610, Mitsubishi chemical cooperation).

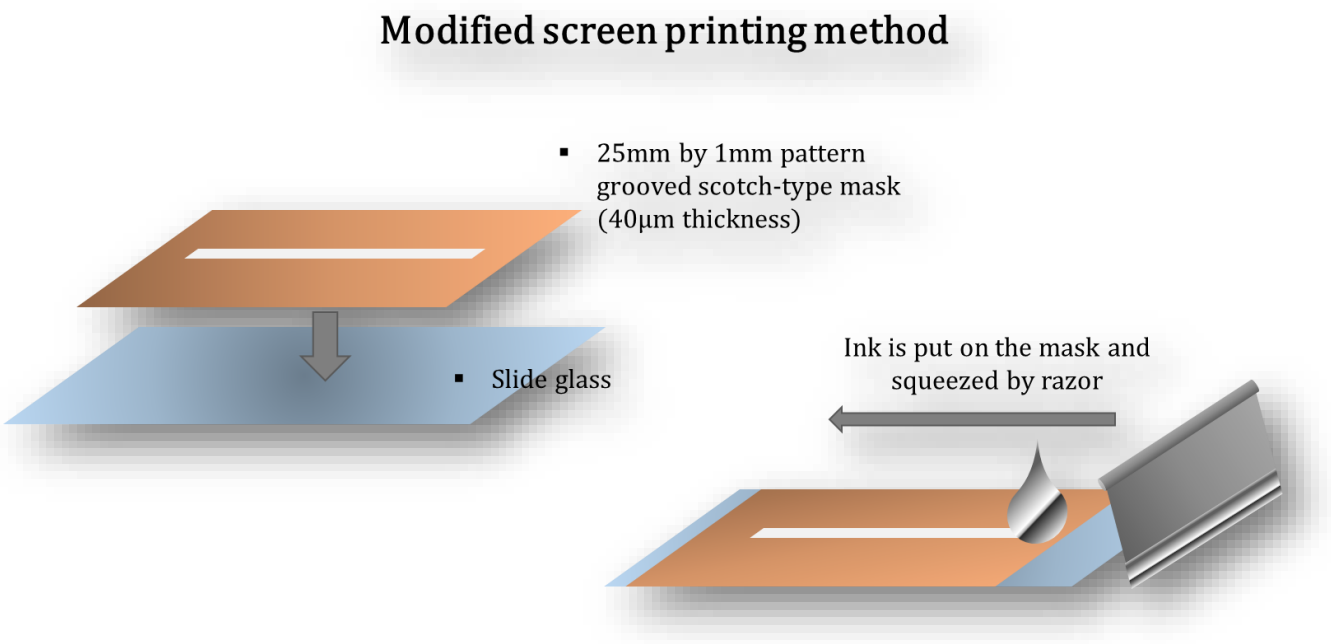

Figure 3.2. Schematic process of modified screen printing method.

3.3. Results and Discussion.

3.3.1. Synthesis of Silver Particles.

The morphology of the smaller silver particles can be observed in the SEM micrograph provided in figure 3.3. Consequently, their size distribution can be seen in figure 3.4. The particles have a spherical shape with an average particle size of 390nm. The morphology of the intermediate sized silver particles can be observed in the SEM micrograph provided in figure 3.5 and their size distribution can be seen in figure 3.6. They also have a spherical shape with an average particle size of 1.74µm. Therefore, it can be concluded that by adding ammonium solution to the silver nitrate solution, the particle size can be decreased. The two chemical reactions expressed below correspond to the synthesis of the smaller silver particles and intermediate sized particles. During synthesis of the smaller silver particles, ammonium hydroxide produces silver ions then finishes by forming a silver compound. When ascorbic acid was added, the silver compound reduces to silver metal. For the synthesis of the intermediate sized particles, the silver ion reacts with ascorbic acid directly which leads to an increase in particle size.

For small size silver particles:

$$AgNO_3 + 2NH_4OH \rightarrow Ag(NH_3)_2{}^{+} + NO_3{}^{-} + 2H_2O$$

$$2Ag(NH_3)_2{}^{+} + C_6H_8O_6 \rightarrow 2Ag^0 + C_6H_6O_6 + 2H^+$$

For middle size silver particles:

$$2Ag^+ + 2NO_3{}^{-} + C_6H_8O_6 \rightarrow 2Ag^0 + 2NO_3{}^{-} + C_6H_6O_6 + 2H^+$$

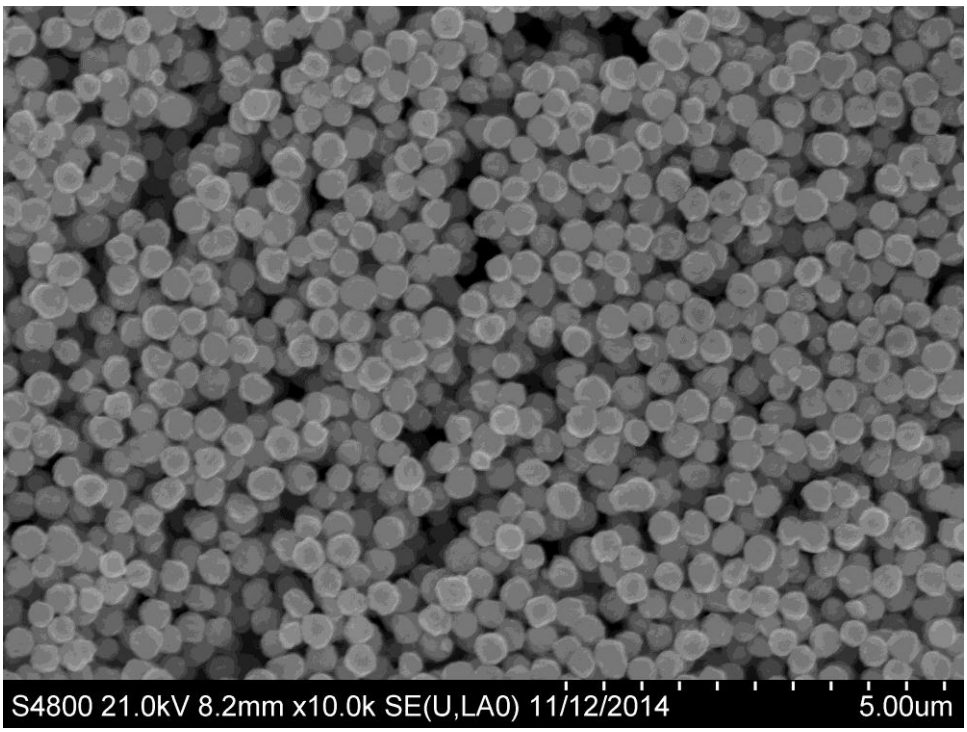

Figure 3.3. SEM Image of Smaller Silver Particles (Average diameter: 390nm).

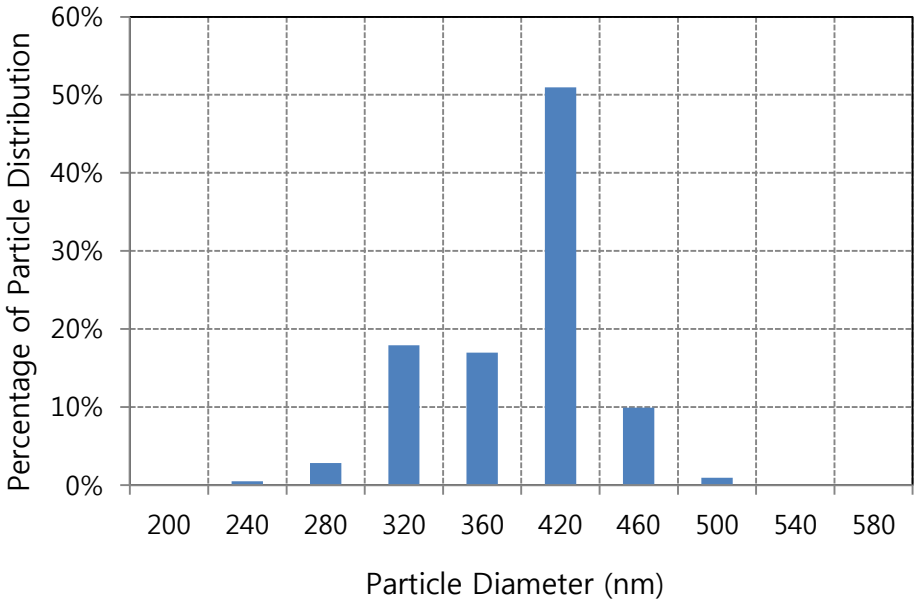

Figure 3.4. Particle Size Distribution of Smaller Silver Particles.

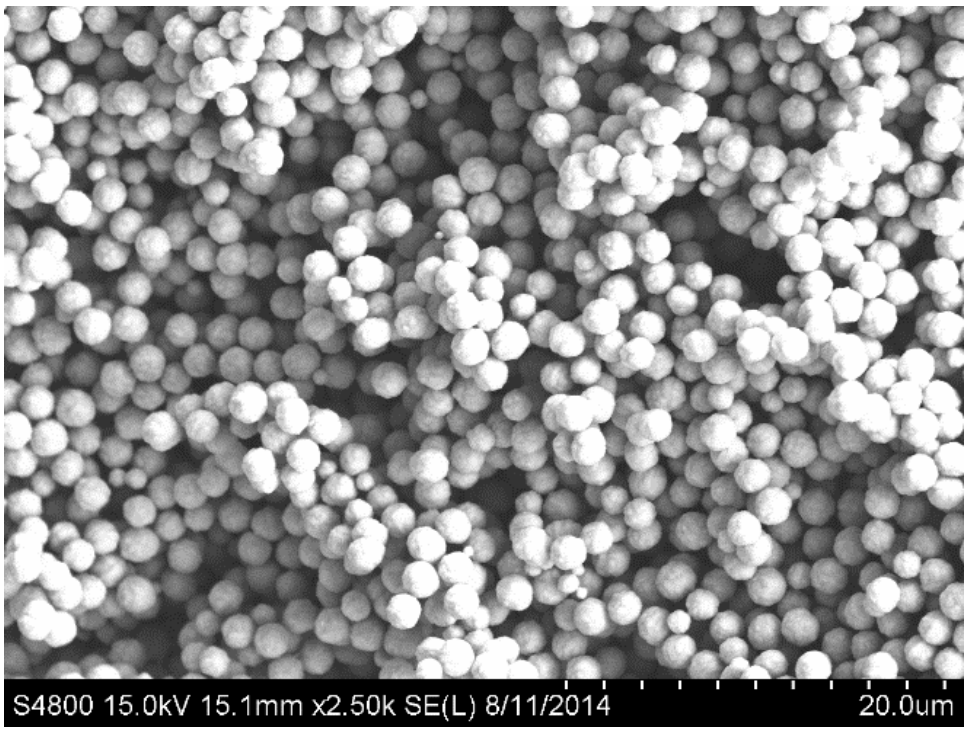

Figure 3.5. SEM Image of Intermediate Sized Silver Particles (Average diameter: 1.74μm).

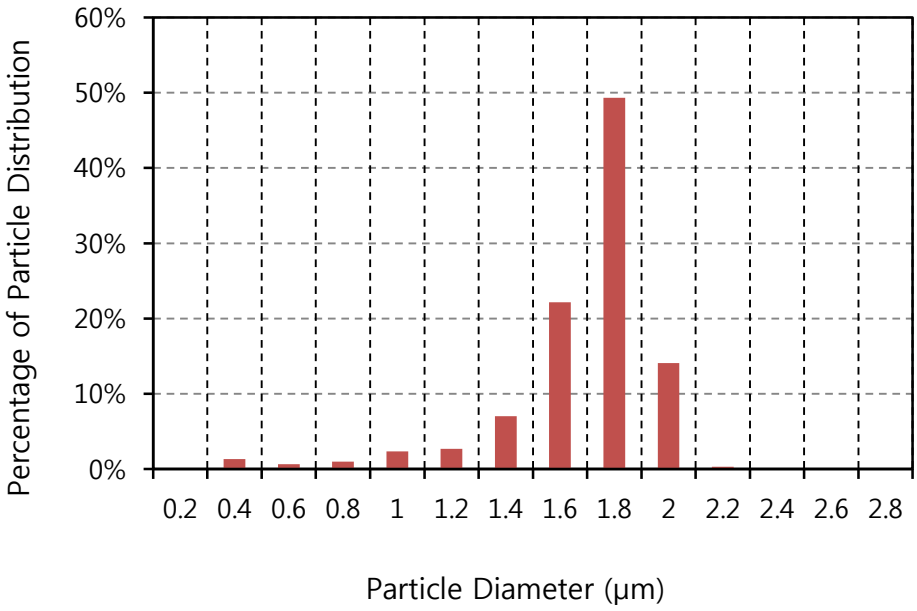

Figure 3.6. Particle Size Distribution of Intermediate Sized Silver Particles.

3.3.2. Synthesis of Cu-Ag Core-shell Particles

Cu-Ag core-shell particles were synthesized using the electro-less plating method. Figure 3.1 shows the theoretical process of such method. However, the silver seeds do not attach easily on the surface of copper particles. Figure 3.7 shows the reaction between the copper particles and silver nitrate (0.38g of copper powder and 0.4g of silver nitrate in 100ml distilled water for 5minutes). It was found through experimental work that the ammonium solution helps to attach the silver seed on the copper particle surface. The silver nitrate concentration is also critical since the silver needs to cover the surface of the copper particle entirely. Figure 3.8 and 3.9 show the effect of different silver nitrate concentration (0.1g and 0.4g respectively) in 98ml of deionized water with 2ml of ammonium solution for the Cu-Ag core-shell particles. The reaction time was 5 minutes. The brighter portion on the particles corresponds to silver and the darker portion on the particle is copper. In figure 3.8, silver does not cover the surface of the copper particle completely. On the other hand, in figure 3.9, the silver covers the copper particle entirely. From these two experimental procedures, it was clear that 0.4g of silver nitrate was the optimal condition to prepare consistent Cu-Ag core-shell particles. The morphology of the intermediate sized silver particles can be observed in the SEM micrograph provided in figure 3.10 and their size distribution can be seen in figure 3.11. They also have a spherical shape with an average particle size of 28.92μm.

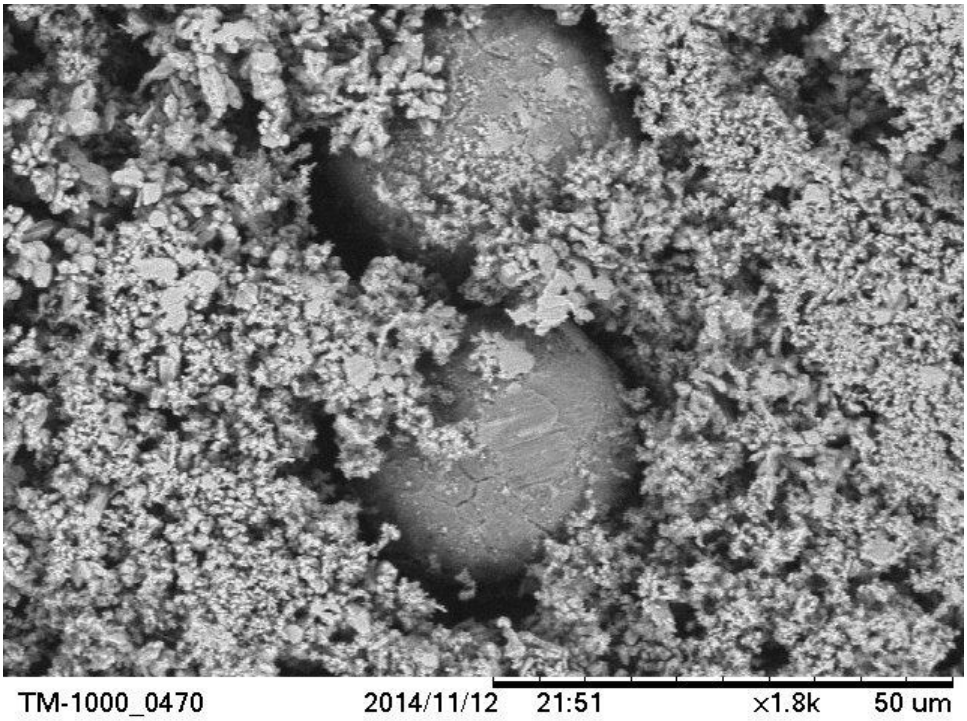

Figure 3.7. SEM Image after Reaction of Copper Particles and Silver Nitrate (Spherical particles: Copper, Flakes: Silver).

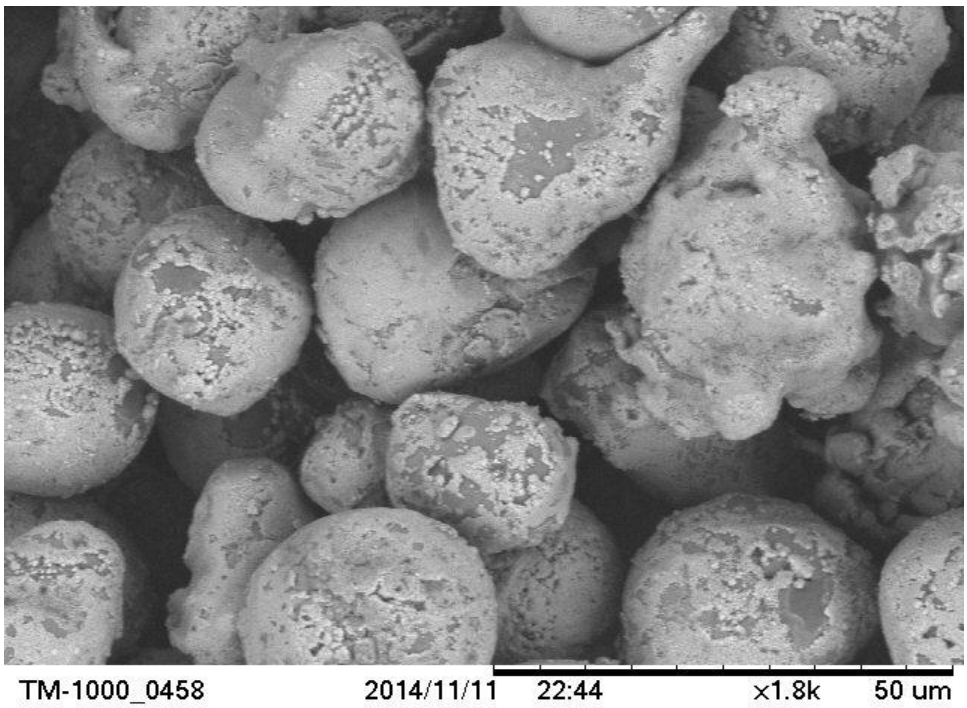

Figure 3.8. SEM Image of Cu-Ag Core-shell Particles (0.1g of Silver Nitrate).

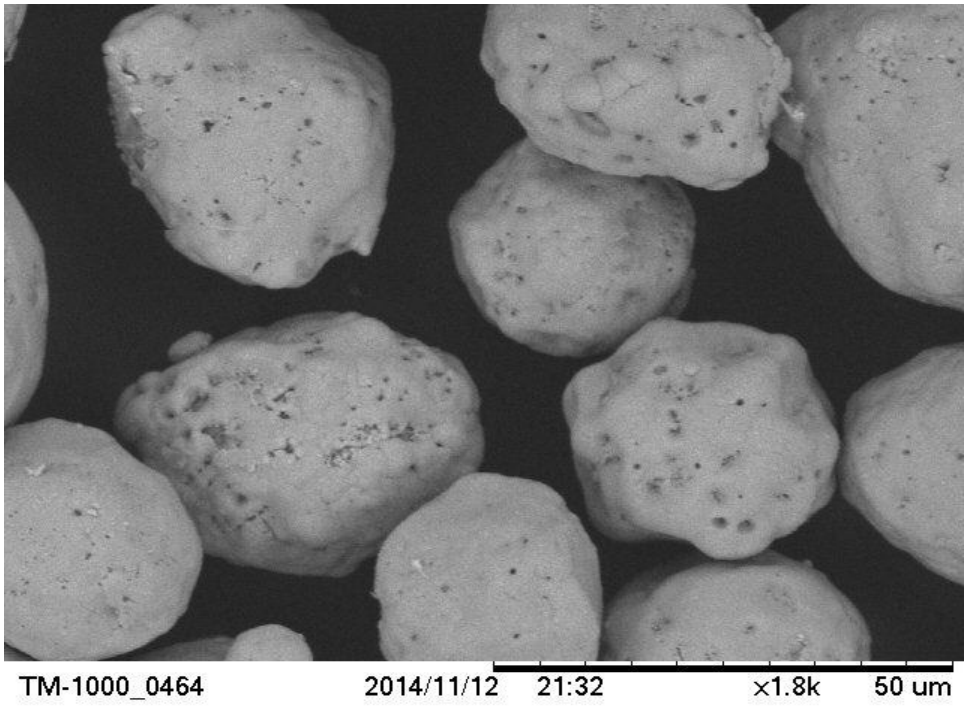

Figure 3.9. SEM Image of Cu-Ag Core-shell Particles (0.4g of Silver Nitrate).

Figure 3.10. SEM Image of Large Cu-Ag Core-shell Particles (Average diameter: 28.92μm).

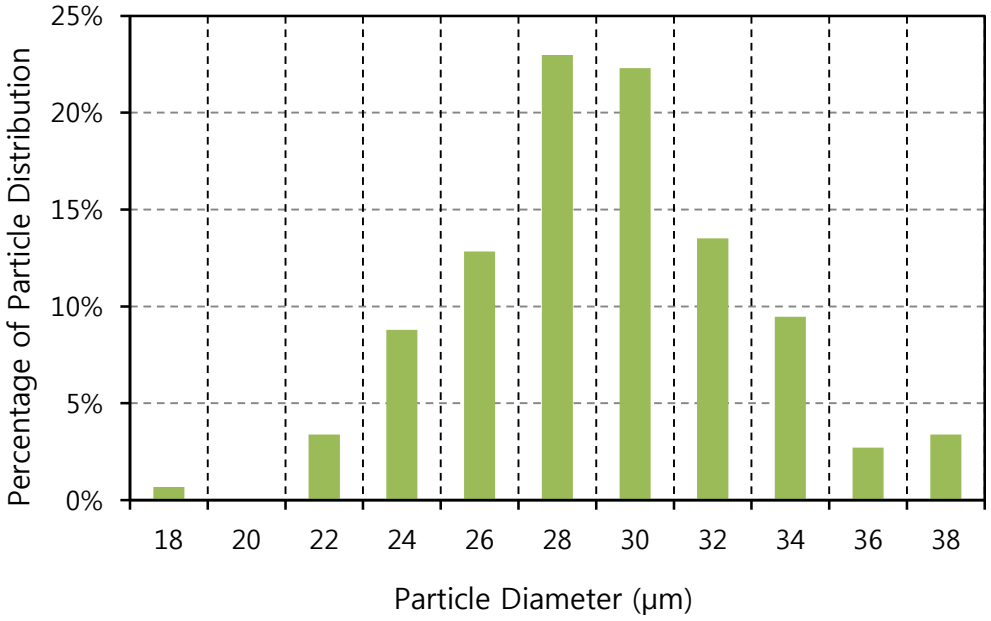

Figure 3.11. Particle Size Distribution of Large Cu-Ag Core-shell Particles.

3.3.3. Fabrication of Silver Electrode.

Three different sized particles (bigger to smaller) were synthesized with an average diameter of 28.92μm, 1.74μm, and 390nm, respectively. According to table 2.3, their size ratio is approximately 25:2.5:0.5. The target portion of the computer simulation results are seen below:

Particle size			Number of particles(S.D.)		
r_1	r_2	r_3	r_1	r_2	r_3
25	**2.5**	**0.5**	**58** (2.66)	**4033** (139.09)	**44130** (1031.44)

According to the simulation results, three different types of silver inks were made. The first ink contained only bigger particles with the binder. The second ink contained both the bigger and the intermediate sized particles. Finally, the third ink contained all three of the particles made (the bigger, the intermediate, and the smaller sized particles). The metal content of the inks are listed in the table 3.2 using the formula shown below.

$$\frac{4}{3}\pi r^3 \times n \times d$$

r: particle size (25, 7.5, and 0.5)
n: number of particles (60, 402, and 55666)
d: silver density

Table 3.2. The Composition of Three Different Kinds of Silver Ink.

	Particles size				
	large	middle	small	Binder	Metal contents
First ink	1g	-	-	0.34g	74.6wt%
Second ink	1g	0.08g	-	0.34g	76wt%
Third ink	1g	0.08g	0.006g	0.34g	76.2wt%

After fabricating the silver electrodes using the modified screen printing method with the three silver inks, the electrodes were sintered at 500˚C for 2 hours. Figures 3.12-17 show the surface of the silver electrode before the sintering process and after the sintering process. The printed pattern came out as particle monolayer. When the smaller particles were added into the ink, they filled the voids between the larger particles. After sintering, particles were necked to each other resulting in fewer voids. The actual packing densities of the printed electrode were measured directly from the SEM micrographs.

Electrical resistivities, actual packing density, and the theoretical packing density of the printed silver electrodes are shown in table 3.3 and figure 3.18. Electrical resistivity was decreased when introducing the smaller particles. Theoretical packing density from the computer simulation results were 46%, 77%, and 91%, respectively. The actual packing densities from the printed electrodes were 87.6%, 94.8%, and 98.8%, respectively. However, the resistivity results are still compatible according to the theoretical packing density. Even though the packing density of the actual printed electrodes surface did not match exactly with the computer simulation results, we can see a tendency of increase in similar proportion between them. Using three different sized particles in the ink is also useful for the production of printed electrodes. For example: during the fabrication of the 40μm thick silver electrode, using 1μm sized particles, it was not possible to make the ink with an excess of 60wt% metal contents. Comparing surface area in 1g of silver powder between 1μm and 40μm, the surface difference is more than 4 billion times, so using different sized particles is essential to make higher metal content silver ink.

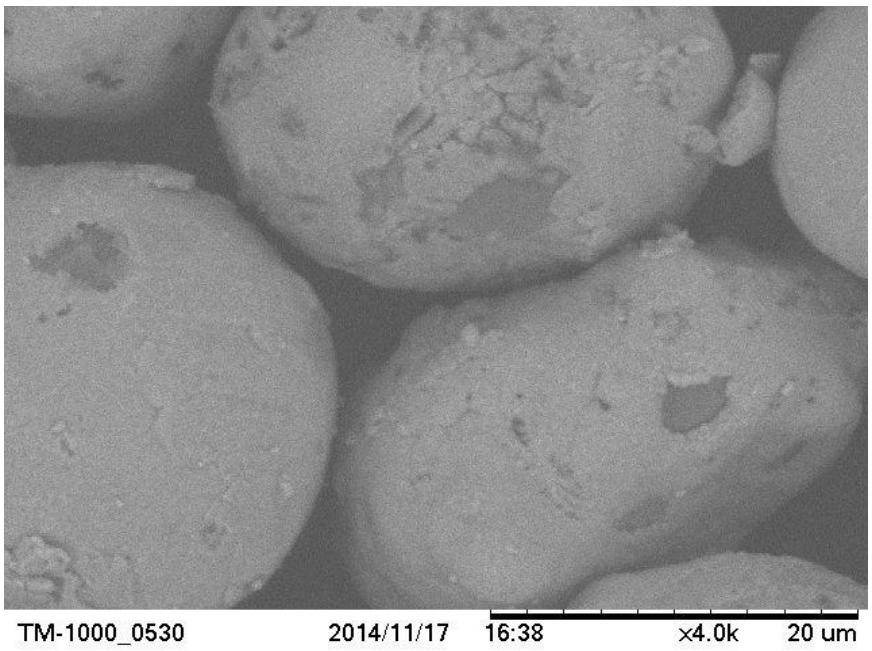

Figure 3.12. Surface of Silver Electrode Using The First Ink before Sintering.

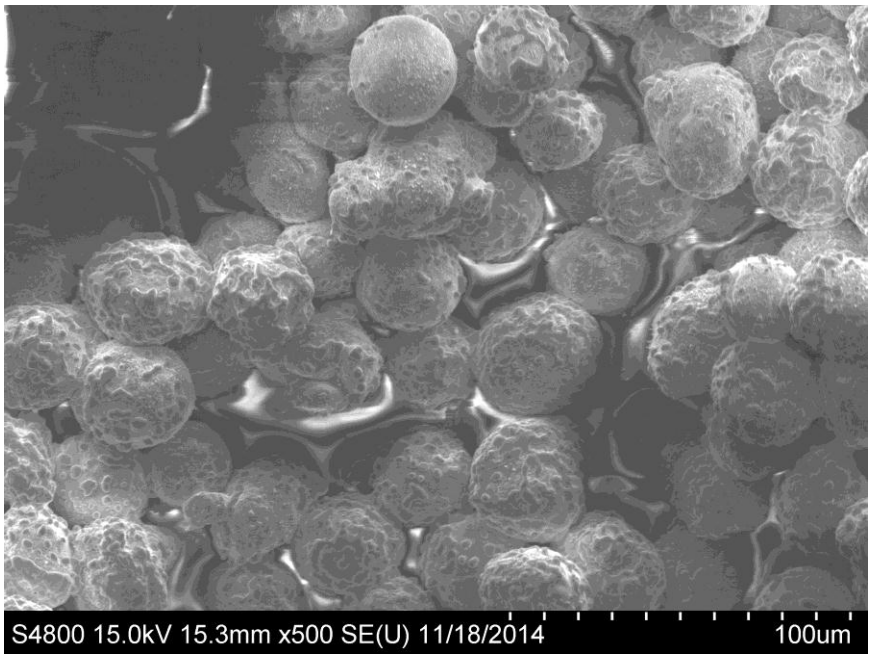

Figure 3.13. Surface of Silver Electrode Using The First Ink after Sintering.

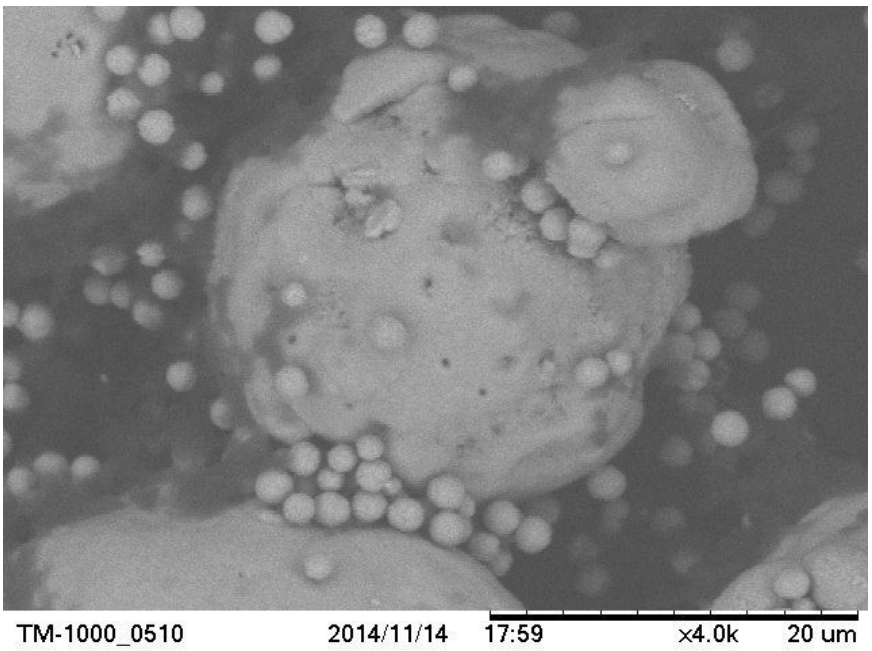

Figure 3.14. Surface of Silver Electrode Using The Second Ink before Sintering.

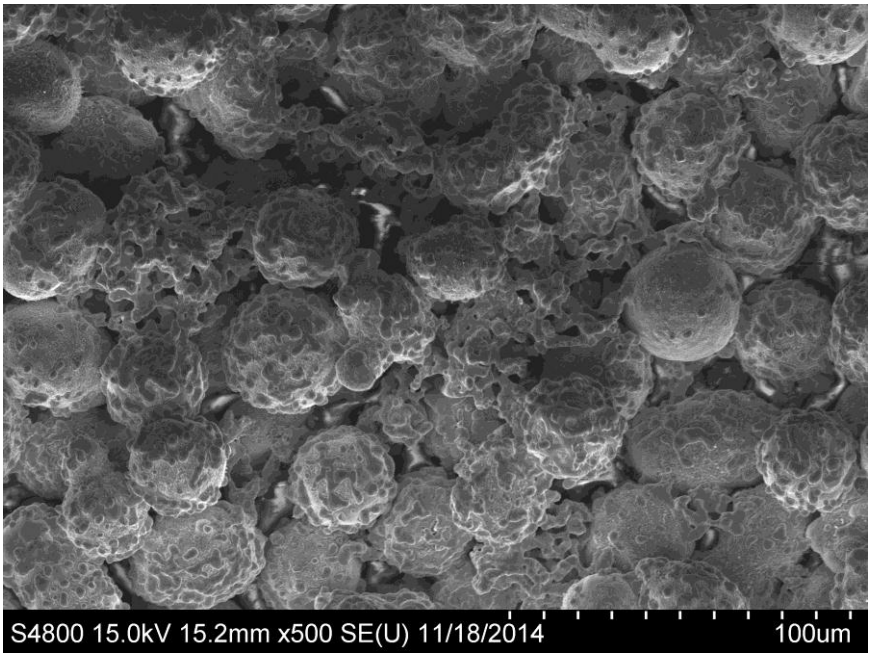

Figure 3.15. Surface of Silver Electrode Using The Second Ink after Sintering.

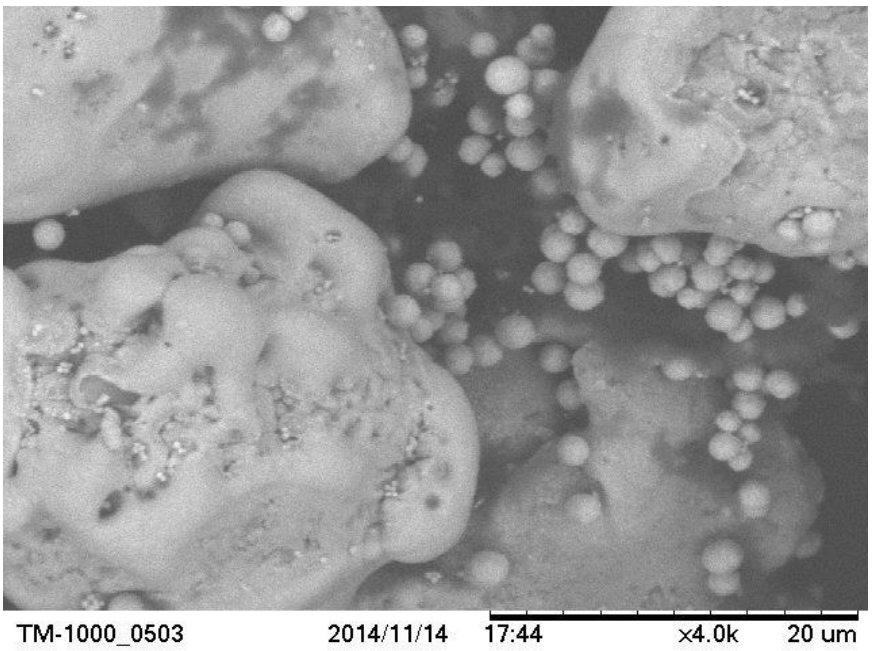

Figure 3.16. Surface of Silver Electrode Made by The Third Ink before Sintering.

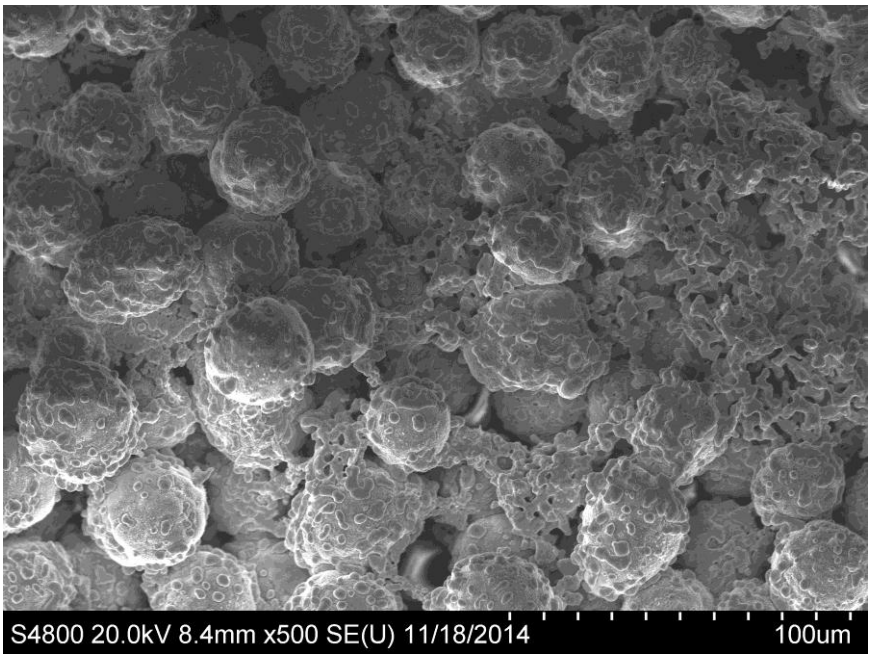

Figure 3.17. Surface of Silver Electrode Made by The Third Ink after Sintering.

Table 3.3. Electrical Resistivities and packing densities of Printed Electrodes.

Silver ink	Metal contents (wt%)	Theoretical packing density (%)	Actual packing density (%)	Electrical resistivity(Ω·cm)
First ink	74.6	46	87.6	$8.71*10^{-2}$
Second ink	76	77	94.8	$4.40*10^{-2}$
Third ink	76.2	91	98.8	$2.96*10^{-2}$

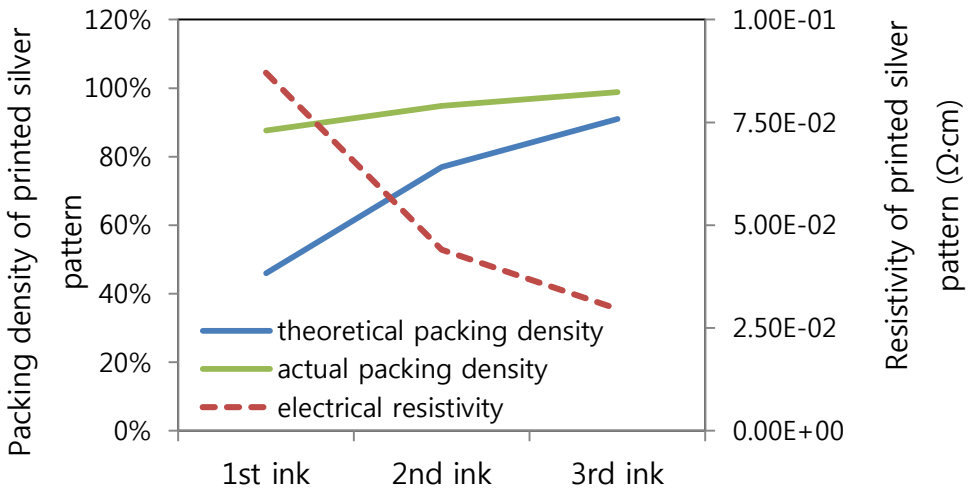

Figure 3.18. Tendency of Electrical Resistivity According to the Packing Density.

Chapter 4

Conclusion

In this study, a simulation program was used with a supercomputer to shorten operation time and result accuracy when calculating packing density of tertiary particles. Thanks to this operation time reduction, complex operations with high Repeating Counts were possible allowing for a higher Packing Factor and a decrease in void space. Additionally, by integrating more CPUs into the simulation, we can obtain a more efficient operation. By obtaining various results using different simulating conditions, we allow a more quantitative experiment to be possible on different viscosity nanoinks. Additionally, we can expect a more broad application of this experimental method in the future. For example, the particle sizes can vary according to the properties of matter when producing a mixture containing several particles.

In order to prove computer simulation results, two different sized silver particles and Cu-Ag core-shell particles were synthesized by wet method and electro-less plating. Three different kinds of silver inks were fabricated, printed, and sintered. The electrical resistivity was decreased when the theoretical and actual packing density were increased.

The packing density of the actual printed electrodes surface did not matched exactly with computer simulation results, however, there were tendency of increase in similar proportion between actual packing density theoretical packing density.

References

[1] J. R. Greer and R. A. Street, “Thermal cure effects on electrical performance of nanoparticles silver inks,” *Acta Materialia* 55 (2007): 6345-6349.

[2] C. L. Lee, K. C. Chang, and C. M. Syu, “Silver nanoplates as inkjet ink particles for metallization at a low baking temperature of 100°C,” *Colloids and Surfaces A: Physicochem. Eng. Aspects* 381 (2011): 85-91.

[3] X. Nie, H. Wang, J. Zou, “Inkjet printing of silver citrate conductive ink on PET substrate,” *Applied Surface Science* 261 (2012): 554-560.

[4] ScienceDaily. "Inkjet printing could change the face of solar energy industry," Accessed September 8, 2014, www.sciencedaily.com/releases/2011/06/110628133022.htm

[5] OPTOMEC. “Printed Antennas,” Accessed September 8, 2014, www.optomec.com/additive-manufacturing/printed-electronics/aerosol-jet-core-applications/printed-antennas/

[6] M. Kimura and T. Nezu, “First Appearance in E-Books, Lighting,” *Nikkei Electronics Asia Magazine*, January, 2010

[7] nScrypt. “Smart pump features,” Accessed September 8, 2014, http://nscrypt.com/direct-print-smartpump/index.php

[8] Displaybank: Technology trend analysis and market prospect of printed electronics 2011~2020 (Displaybank Co., Ltd, 2011)

[9] C. Buzea, I. Pacheco, and K. Robbie, "Nanomaterials and Nanoparticles: Sources and Toxicity," *Biointerphases* 2 (2007): MR17–MR71.

[10] S. Zeng, D. Baillargeat, H.-P. Ho, and K.-T. Yong, "Nanomaterials enhanced surface plasmon resonance for biological and chemical sensing applications," *Chemical Society Reviews* 43 (2014): 3426–3452.

[11] P. Buffat and J. P. Borel, “Size effect on the melting temperature of gold particles,” *Physical Review A* 13(1976): 2287-2298.

[12] K. Han and N. Kim, “Challenges and Opportunities in Direct Writing Technology Using Nano-metal Particles,” *KONA Powder and Particle Journal* 27 (2009): 73-83.

[13] N. Kim, A. Amert, S. Woessner, S. Decker, S. Kang, and K. Han, “Effect of Metal Poder Packing on the Conductivity of Nanometal Ink,” *Journal of Nanoscience and Nanotechnology* 7 (2007): 3909-3905.

[14] K. Sobolev and A. Amirjanov, "The Development of a Simulation Model of the Dense Packing of Large Particulate Assemblies," *Powder Technology* 141 (2004): 155-160.

[15] D. A. Robinson and S. P. Friedman, "Electrical Conductivity and Dielectric Permittivity of Sphere Packing: Measurements and Modeling of Cubic Lattices, Randomly Packed Monosize Spheres and Multi-size Mixtures," *physica A* 358 (2005): 447-465.

[16] M. Gan, N. Gopinathan, X. Jia, and R. A. Williams, "Predicting Packing Characteristics of Particles of Arbitrary Shapes," *KONA* 22 (2004): 82-93.

[17] A. K. Amert, D. Oh, and N. Kim, "A Simulation and Experimental Study on Packing on Nano-inks to Attain Better Conductivity," *Journal of Applied Physics* 108 (2010): 102806.

[18] Z. P. Zhang, L. F. Liu, Y. D. Yuan, and A. B. Yu, "A Simulation Study of the Effects of Dynamic Variables on the Packing of Spheres," *Powder Technology* 116 (2001): 23-32.

[19] Y. F. Chenf, S. J. Guo, and H. Y. Lai, "Dynamic Simulation of Random Packing of Spherical Particles," *Powder Technology* 107 (2000):123-130.

[20] R. P. Zou, J. Q. Xu, C. L. Feng, A. B. Yu, S. Johnston, and N. Standish, "Packing of Multi-Sized Mixtures of Wet Coarse Spheres," *Powder Technology* 130 (2003): 77-83.

[21] K. Sobolev and A. Amirjanov, "A Simulation Model of the Dense Packing of Particulate Materials," *Advanced Powder Technology*, 15(2004): 365-376.

[22] S. Siiria and J. Yliruusi, "Particle Packing Simulation Based on Newtonian Mechanics," *Powder Technology* 174 (2007): 82-92.

[23] A. R. Riyadh and A. Mustafa, "Simulation of Random Packing of Polydisperse Paricle," *powder Technology* 176 (2007): 47-55.

[24] H. Jung, H. Ko, S. Kim, "Large amounts of data Processing by using Supercomputer," *Trans. of the KIIT* (2009): 487-491.

[25] H. Borsook and G. Keighley, "Oxidation-Reduction Potential of Ascorbic Acid (Vitamin C)," Physiology 19 (1933): 875-878.

[26] G. O. Mallory and J. B. Hajdu, trans., Electroless Plating (American Electroplaters and Surface Finishers Society, INC., 1990), 1-6.

Curriculum Vita

Kyungdeok Jang was born in Seoul, South Korea. The second son of Jusin Cho and Taegeun Jang, he graduated from Kyeongseong High School, Seoul, South Korea. In spring 2008, Kyungdeok entered Seokyeong University, Seoul, South Korea. While pursuing a bachelor's degree in Chemical and Biological Engineering, he worked as a research assistant in Korea Environment and Nano Research Center, during 2010-2012 he published two journal papers as a first author, registered one patent. After receiving his bachelors of science in 2012, he enrolled in graduate school at the University of Texas at El Paso as an international student. During his master program in Department of Metallurgical and Materials Engineering, Kyungdeok Jang published two papers as a first author and coauthor, and he has won "Challenge Round 2 Student Track Award" from Paso Del Norte Venture Competition in 2013 about the urban mining technology and "Graduate Research Award" from Department of Metallurgical and Materials Engineering in 2014.

Permanent Address: 304-504
60, Taebong-ro 2-gil, Seocho-gu,
Seoul, 137-140, South Korea
Or
playzanggu@gmail.com